Effect of Structural Dynamics on the Opto-Electronic Properties of Bare and Hydrated ZnS QDs

ARTICLE *in* THE JOURNAL OF PHYSICAL CHEMISTRY C · JANUARY 2014

Impact Factor: 4.77 · DOI: 10.1021/jp409182r

4 AUTHORS, INCLUDING:

Jon Mikel Azpiroz
Italian National Research Council
21 PUBLICATIONS **142** CITATIONS
SEE PROFILE

Filippo De Angelis
Università degli Studi di Perugia
264 PUBLICATIONS **11,196** CITATIONS
SEE PROFILE

THE JOURNAL OF PHYSICAL CHEMISTRY C

Article

pubs.acs.org/JPCC

Effect of Structural Dynamics on the Opto-Electronic Properties of Bare and Hydrated ZnS QDs

Jon M. Azpiroz,[†] Edoardo Mosconi,[‡] Jesus M. Ugalde,[†] and Filippo De Angelis*[,‡]

[†]Kimika Fakultatea, Euskal Herriko Unibertsitatea (UPV/EHU) and Donostia International Physics Center (DIPC), P.K. 1071 Donostia, Euskadi, Spain

[‡]Computational Laboratory for Hybrid/Organic Photovoltaics (CLHYO), Istituto CNR di Scienze e Tecnologie Molecolare (ISTM-CNR), via Elce di Sotto 8, 1-06123, Perugia, Italy

Supporting Information

ABSTRACT: Quantum mechanical calculations on the structural and optoelectronic features of two realistic wurtzite-like ZnS quantum dot (QD) models, namely, $(ZnS)_{33}$ and $(ZnS)_{116}$, are presented both in vacuo and in an explicit water solution environment. Car−Parrinello molecular dynamics (CPMD) simulation and excited-state, Time-Dependent Density Functional Theory (DFT/TDDFT) calculations on extended models are combined to unravel hitherto inaccessible atomistic features of the investigated systems. Ultrasmall QDs are predicted to exhibit strong dynamical fluctuations. Accordingly, the bare $(ZnS)_{33}$ model undergoes a drastic structural rearrangement and evolves from the starting bulk-like structure to an amorphous phase. The geometrical changes occurring over the time are reflected on the opto-electronic properties. The band-edge states and the optical absorption onset both sizably vary along the CPMD trajectory. Eventually, the optical gap decreases due to the emergence of high-lying occupied orbitals. These midgap states are mainly localized in undercoordinated S sites and could act as trap states for the photogenerated holes. Water molecules are predicted to form strong $Zn-OH_2$ bonds with the surface Zn atoms. Hydration seems to lower the surface energy, stabilize the wurtzite polymorph, hinder the Zn−S bond breaking, and largely prevent the appearance of trap states. Besides, adsorbed water molecules produce a notable blue-shift of the optical gap. The electrostatic field induced by the solvent shell and the electron-donor properties of the water molecules are supposed to be responsible for the opening of the gap. Moreover, capping the QDs with water molecules increases the intensity of the lowest-lying electronic excitations. This study sheds light on the important opto-electronic modifications occurring for realistic QD in water solution and offers at the same time the methodological framework to investigate photocatalytic reactions mediated by ZnS.

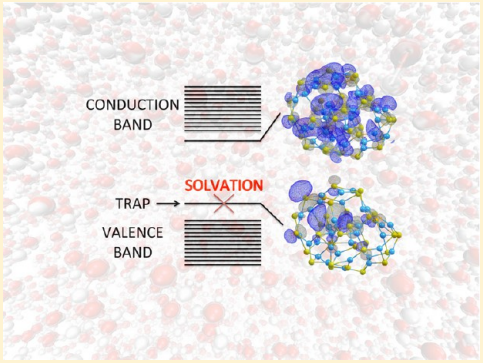

1. INTRODUCTION

Over the last years, interest on II−VI (II: Zn, Cd, Hg; VI: O, S, Se, Te) semiconductor quantum dots (QDs) has grown notably due to their novel properties.[1,2] Their unique behavior, which often differs from the bulk material, lies on the combined effect of their large surface-to-volume ratio and quantum confinement. Due to their outstanding properties, they are recurrently employed as solar cell components,[3,4] optical sensors,[5,6] optoelectronic devices,[7] and photocatalysts.[8−11]

Among the II−VI materials, ZnS nanostructures have earned lots of attention. ZnS QDs, typically absorbing/emitting in the UV−vis, have found application in opto-electronics[12] and catalysis.[13] Besides, since ZnS is an abundant, highly stable, and environmentally friendly material, ZnS nanoparticles are amenable for biological applications.[14]

Due to the high surface-to-volume ratio inherent in nanomaterials, surface ligands and solvent molecules may play an important role on the properties of QDs.[15] Capping molecules are known to modify the surface energy of QDs and determine, to some extent, the atomic arrangement of the nanomaterial. Moreover, surface adsorbed molecules tailor the opto-electronics of QDs. In this context, interest on hydrated ZnS QDs has increased notably.[16−20] Indeed, most of the QDs operate in water or, at least, immersed in a solvent. The understanding of ZnS−water interaction is thus particularly important with a view to their (bio)medical application. Even if ZnS QDs have been employed themselves in biology, ZnS is also commonly used as protective shell for CdSe QDs to avoid the release of toxic Cd^{2+} ions. Therefore, for a safe application of ZnS nanostructures in vivo, their behavior in water solution should be precisely investigated. From a different perspective, the study of the ZnS−water interaction may pave the way to understand the photocatalytic water splitting reaction occurring at the semiconductor surfaces. Recently, ZnS QDs have proven to be an efficient catalyst for H_2 generation from water.[21,22]

Received: September 13, 2013
Revised: December 17, 2013
Published: January 18, 2014

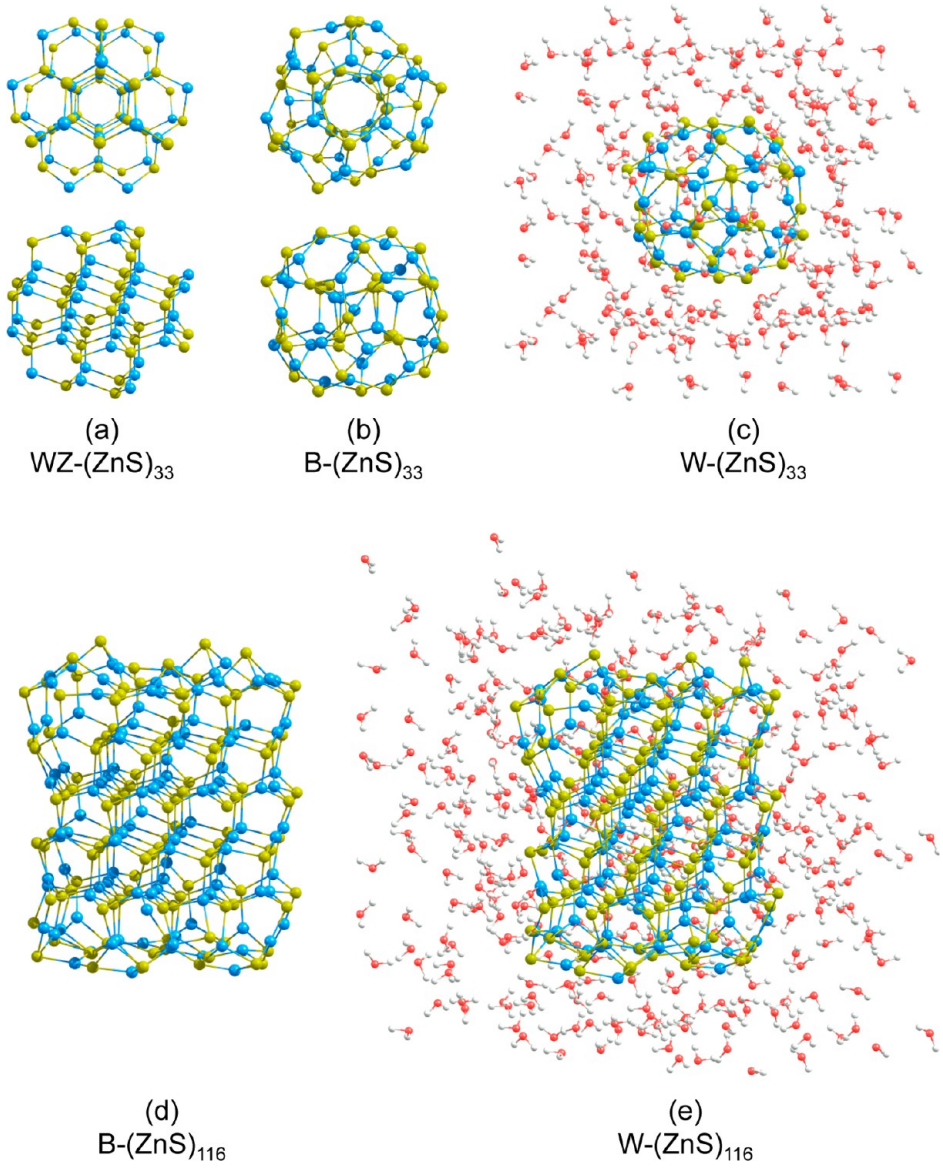

Figure 1. (a) Geometry of the pristine WZ-$(ZnS)_{33}$ cluster as cleaved out from bulk wurtzite. (b) Optimized geometry of the bare B-$(ZnS)_{33}$. (c) Starting geometry of the hydrated W-$(ZnS)_{33}$ for the CPMD simulation. (d) Optimized geometry of the bare B-$(ZnS)_{116}$. (e) Starting geometry of the hydrated W-$(ZnS)_{116}$ for the CPMD simulation. Light blue = Zn, yellow = S, red = O, and white = H atoms.

Most of the works published so far on hydrated ZnS QDs have focused on the effect of water (and other capping ligands) on the structure of the QDs.[16−20] In these studies, the uncapped ZnS QDs are reported to undergo a drastic rearrangement driven by the unsaturated atoms on the surface. Surface ligands are known to cap undercoordinated atoms, minimize surface energy, and stabilize the QD structure. These conclusions are based on various experimental techniques but also assisted by classical molecular dynamics simulations. Ab initio molecular dynamics, which provide an accurate framework for the description of intermolecular forces, have been limited to minimal models such as $(ZnS)_4$.[20] For this kind of small clusters, $(ZnS)_n$, with n = 4, 6, 12, the effect of the surrounding water molecules on the opto-electronic properties have been investigated by means of DFT/TDDFT calculations.[23,24] So far computational modeling has provided valuable insights of the effect of hydration on the structural and the optoelectronic properties of ZnS QDs. Realistic models have however been analyzed only by means of classical molecular dynamics simulations. Then, accurate DFT/TDDFT calculations have been reported for realistic $(ZnS)_{116}$ clusters of nanometric size but the effect of the water solvent was described by an implicit solvation model.[25] Furthermore, previous studies have been carried out on optimized minimum energy structures, thus not accounting for the dynamic behavior of solvated QDs. Experimentally, however, QDs may display a marked dynamical character and structural changes are reflected on the absorption and emission features, which change over time.[26] The interplay between the structure and the ligands in relation to the presence of trap states (hole or electron) is also of particular interest.[27,28]

The present work represents a step forward in the characterization of hydrated ZnS QDs. It tries to unveil the role of structural fluctuations and solvent effects on the opto-electronic properties of realistic QDs. With that goal, two wurtzite-like QD models of increasing size have been selected, $(ZnS)_{33}$ and $(ZnS)_{116}$, surrounded by shells of 207 and 341 explicit water molecules, respectively, see Figure 1. Ab initio

dx.doi.org/10.1021/jp409182r | J. Phys. Chem. C 2014, 118, 3274−3284

molecular dynamics simulations in the Car−Parrinello framework have been performed to capture the dynamic fluctuations of the bare and hydrated QDs. Furthermore, the ground and excited state of an ensemble of configurations sampled along the dynamics have been characterized by hybrid DFT/TDDFT calculations.

Water has been predicted to stabilize wurtzite bulk-like structures, even for small ZnS QDs, which would otherwise be disordered in nature. Furthermore, the presence of surrounding water molecules sizably affects the electronic and optical features of the models studied, leading to a strong reduction in the number of midgap states, which could act as charge trapping sites. This work sheds light on the important optoelectronic modifications occurring for realistic QD in water solution and provides the methodological framework to investigate photocatalytic reactions mediated by ZnS.

2. MODEL AND COMPUTATIONAL DETAILS

To unravel the behavior of hydrated ZnS nanostructures two realistic models of increasing size have been chosen, namely $(ZnS)_{33}$ and $(ZnS)_{116}$. With an approximate diameter of 1 nm, the $(ZnS)_{33}$ cluster is a recurrent product of both gas and condensed phase synthesis of ZnS nanostructures.[29] To explain the abundance of the so-called magic $(ZnS)_{33}$ stoichiometry, found for other II−VI materials like ZnSe, CdS, and CdSe,[29] two kind of models have been proposed: (1) core@cage[29−31] and (2) wurtzite-like.[32,33] In this work, the latter has been chosen. However, as one may notice from Figure 1, the relaxed structure (b) significantly differs from the pristine cluster (a) cleaved from the bulk wurtzite. Such reconstruction (or self-healing, as named by Puzder et al.[33]) minimizes the number of dangling bonds on the surface. To provide a direct comparison with the experimentally accessible ZnS QDs, the 1.5 nm size $(ZnS)_{116}$ model has also been considered. Sliced from the bulk wurtzite, Zn and S adatoms have been placed on its S- and Zn-rich polar faces, leading to the saturation of the undercoordinated atoms, the minimization of the dipole along the *c* axis, and the stabilization of the pristine bulk-like nanoparticle.[25] The gas phase optimized structures of the $(ZnS)_{33}$ and $(ZnS)_{116}$ clusters, obtained by means of the PBE functional[34] in combination with a STO valence DZ basis set, as implemented in the ADF 2012.10 software,[35] have been immersed in a periodic box of water molecules, and ab initio Car−Parrinello molecular dynamics (CPMD) have been performed on the resulting fully solvated systems. For comparison, the dynamics of the bare $(ZnS)_{33}$ cluster have also been studied.

CPMD simulations[36] have been carried out using the GGA-PBE exchange-correlation functional[34] in conjunction with a plane wave basis set (25/240 Ry cutoff for wave functions and augmented charge density) and ultrasoft pseudopotentials,[37] as implemented in the Quantum-Espresso package.[38] Dynamic simulation have been performed at finite temperature (350 K), in a cubic supercell of side 16.78, 19.71, and 24.83 Å for the bare $(ZnS)_{33}$, the hydrated $(ZnS)_{33}(H_2O)_{207}$, and the hydrated $(ZnS)_{116}(H_2O)_{341}$ models, respectively. The number of water molecules included in the simulation has been evaluated by considering the volume encumbrance of the cluster. In particular, starting from a preliminary simulation of bulk water, a cavity is created removing a number of water molecules equivalent to the volume of the cluster, and finally, the cluster is placed into the cavity. In order to equilibrate the systems, they are allowed to evolve for 1 ps to check their actual temperature and then a Nosé thermostat is applied for about 2 ps. Once the thermalization is achieved, the thermostat is removed and the systems are allowed to evolve naturally in time.

The total simulation time was about 12 ps for the bare $(ZnS)_{33}$ cluster and about 6 ps for the hydrated $(ZnS)_{33}$ model, composed by 687 atoms. For the hydrated $(ZnS)_{116}$ cluster, comprising a total of 1255 atoms, the atomic motion was evolved for about 4 ps. Interestingly, for the hydrated $(ZnS)_{33}$ cluster the statistics at 4 and 6 ps are almost indistinguishable, validating the shorter simulation time for the $(ZnS)_{116}$ model, see Figure S3, Supporting Information.

For the bare and hydrated $(ZnS)_{33}$ models, snapshots were taken each 200 time steps (ca. 0.05 ps) and DFT/TDDFT calculations were performed on top of them employing the modified form of the B3LYP functional, including 27.5% of HF exchange (B3LYP* hereafter), in conjunction with the LANL2DZ[39−41] basis set. Due to the very large size of the hydrated $(ZnS)_{116}$ model, only single point calculations were conducted on a few representative snapshots taken from the dynamics. In previous works on II−VI semiconductor nanostructures, the parametrization of B3LYP has led to a better description of the optoelectronic properties.[25,42−44] Regarding the basis set, LANL2DZ is probably the most popular choice to model realistic II−VI nanoclusters because it reproduces the results of larger sets at a fraction of the computational cost. Quite recently, however, it has been shown to perform quite disappointingly for II−VI QDs.[45,46] To check the reliability of LANL2DZ for our purposes, it has been benchmarked against other basis sets such as SDD,[47,48] def2-SVP,[49,50] and the reference def2-TZVP,[49,50] see Figure S4, Supporting Information. The conductor-like polarizable continuum model of solvation (CPCM) has also been employed.[51−53] All the DFT/TDDFT calculations have been conducted by means of the Gaussian09 program package.[54]

Radial distribution functions have been calculated using the Virtual Molecular Dynamics (VMD) software.[55] The X-ray diffraction patterns have been simulated by means of the Mercury software package.[56] To do so, the models have been placed in a 10 nm long cubic unit cell. In order to reproduce the experimental conditions, the X-ray wavelength has been set to the Cu Kα value of 0.154056 nm. A fwhm of 0.1° has been chosen for the convolution of the diffractogram.

3. RESULTS AND DISCUSSION

3.1. Structural Features. The CPMD simulations reveal that the B-$(ZnS)_{33}$ model undergoes a significant reconstruction. Along the dynamics it evolves from the wurtzite-like geometry to an amorphous structure. After local geometry optimization, the amorphous structure was calculated to lie about 20 kcal/mol lower than the optimized bulk-like geometry.[57] It appears that ultrasmall nanoclusters are intrinsically disordered, in agreement with the experimental evidence.[26] So far, such small QDs have been predicted to adopt ordered structures such as bulk- or core@shell-like.

With the increasing size of the nanostructure (and the decreasing surface-to-volume ratio), bulk-like geometries are expected to be favored. In this sense, based on CPMD calculations, the bare $(ZnS)_{116}$ model was predicted to preserve the wurtzite structure, though surface atoms were found to rearrange during the dynamics.[25] Apparently, the inclusion of explicit solvent stabilizes the bulk-like structure. For the W-$(ZnS)_{33}$ model, the characteristic pattern of the wurtzite structure is recognizable along the whole trajectory.

dx.doi.org/10.1021/jp409182r | J. Phys. Chem. C 2014, 118, 3274−3284

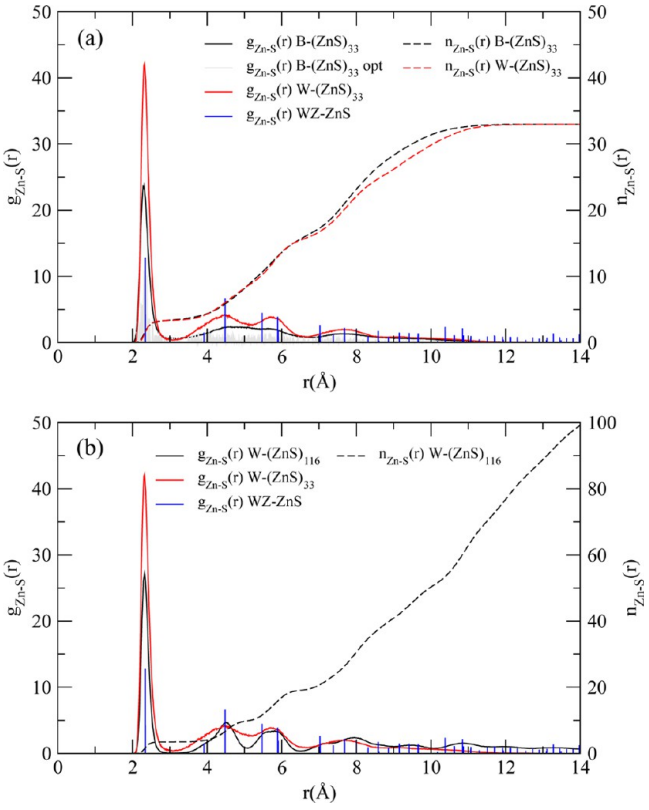

Figure 2. Zn−S radial distribution functions ($g_{Zn-S}(r)$) and coordination numbers ($n_{Zn-S}(r)$) of the B-$(ZnS)_{33}$ (in black), W-$(ZnS)_{33}$, and W-$(ZnS)_{116}$ models (in red), averaged along the CPMD trajectory. For sake of comparison, the RDF of the optimized B-$(ZnS)_{33}$ cluster (in gray) and the RDF of bulk wurtzite ZnS (in blue) are provided.

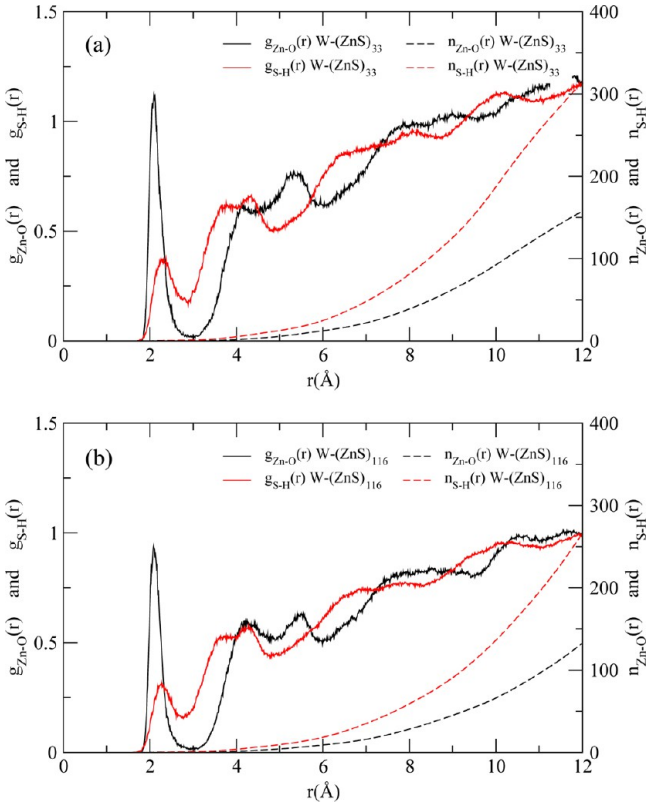

Figure 3. Zn−O and S−H radial distribution functions ($g_{Zn-O}(r)$ and $g_{S-H}(r)$) and coordination numbers ($n_{Zn-O}(r)$ and $n_{S-H}(r)$) of the hydrated W-$(ZnS)_{33}$ (a) and W-$(ZnS)_{116}$ models (b).

To further characterize the structure of our models, the Zn−S radial distribution function (RDF) has been calculated, see Figure 2. For comparison, the Zn−S RDF of the perfect $(ZnS)_{33}$ model (WZ-$(ZnS)_{33}$), as cleaved from the bulk wurtzite, has been also considered. For the latter, Zn−S bond distances are set to the experimental bulk value of 2.35 Å. As one may notice from Figure 2, the time-averaged Zn−S RDFs ($g_{Zn-S}(r)$) of the B-$(ZnS)_{33}$ and W-$(ZnS)_{33}$ models substantially deviate from the pristine WZ-$(ZnS)_{33}$ model. For the latter, the Zn−S RDF displays sharp peaks at well-determined distances, such as the eye-catching feature at 2.35 Å, which corresponds to adjacent Zn and S atoms. According to the CPMD simulations, both models in the gas phase and in water solution exhibit broader peaks due to surface reconstruction and the thermal fluctuations. The first peak is centered at 2.30 and 2.32 Å for B-$(ZnS)_{33}$ and W-$(ZnS)_{33}$, respectively, sligthly shorter than in the bulk ZnS. The longer average Zn−S distance observed for W-$(ZnS)_{33}$ suggests that water adsorption relaxes the shrunk Zn−S bonds in B-$(ZnS)_{33}$. Remarkably, B-$(ZnS)_{33}$ displays a wider distribution of Zn−S distances, indicative of a lower short-range ordering as compared to W-$(ZnS)_{33}$. From the area under the peak, an average Zn−S coordination number of about 3.3 has been obtained for both B-$(ZnS)_{33}$ and W-$(ZnS_{33}$. A similar coordination number of 3.2 has been reported for magic-size $(CdSe)_n$ clusters (n = 33, 34).[29] For r > 3 Å, the B-$(ZnS)_{33}$ model displays a broad profile of Zn−S pair distances, meaning little long-range ordering. On the contrary, the W-$(ZnS)_{33}$ model displays three well-resolved peaks, representing a higher degree of ordering. This finding reveals that the atomic ordering of the cluster increases upon hydration, in agreement with the experimental observations and previous classical MD simulations.[19,20]

For comparison, the Zn−S RDF of the W-$(ZnS)_{116}$ is also reported in Figure 2. The main features already observed for W-$(ZnS)_{33}$ are recognizable. However, the sharpening of the bands mirrors the highly ordered structure of the W-$(ZnS)_{116}$ cluster relative to the small model. Apart from the crystallinity imposed by the solvent, the pristine $(ZnS)_{116}$ undergoes a modest structural distortion upon relaxation, whereas the $(ZnS)_{33}$ model requires a drastic atomic rearrangement to saturate the undercoordinated atoms on the surface. An average bond distance of 2.33 Å is calculated for adjacent Zn and S atoms (vs 2.32 Å in W-$(ZnS)_{33}$), with an average coordination number of 3.4 (vs 3.3 Å in W-$(ZnS)_{33}$). The Zn−S bond length and coordination number increase with the size of the hydrated model, as the surface-to-volume ratio decreases, and swiftly approach the bulk values of 2.35 Å and 4, respectively.

To bridge the gap between our calculations and the experiment, the XRD patterns of our models have been simulated, see Figure S5, Supporting Information. The B-$(ZnS)_{33}$ model displays two broad bands at 2θ = 30 and 50°, in agreement with most of the experiments on ultrasmall II−VI QDs.[58,59] Upon hydration, the diffraction features become sharper, meaning again that surface adsorption induces structural ordering.[60] The acute diffraction signatures found for $(ZnS)_{116}$ reflect the high crystallinity of this system.

To deepen on the dynamics of the investigated models, the number of 2-, 3-, and 4-fold Zn and S atoms have been computed along the CPMD trajectories, see Figure S6 and

dx.doi.org/10.1021/jp409182r | J. Phys. Chem. C 2014, 118, 3274−3284

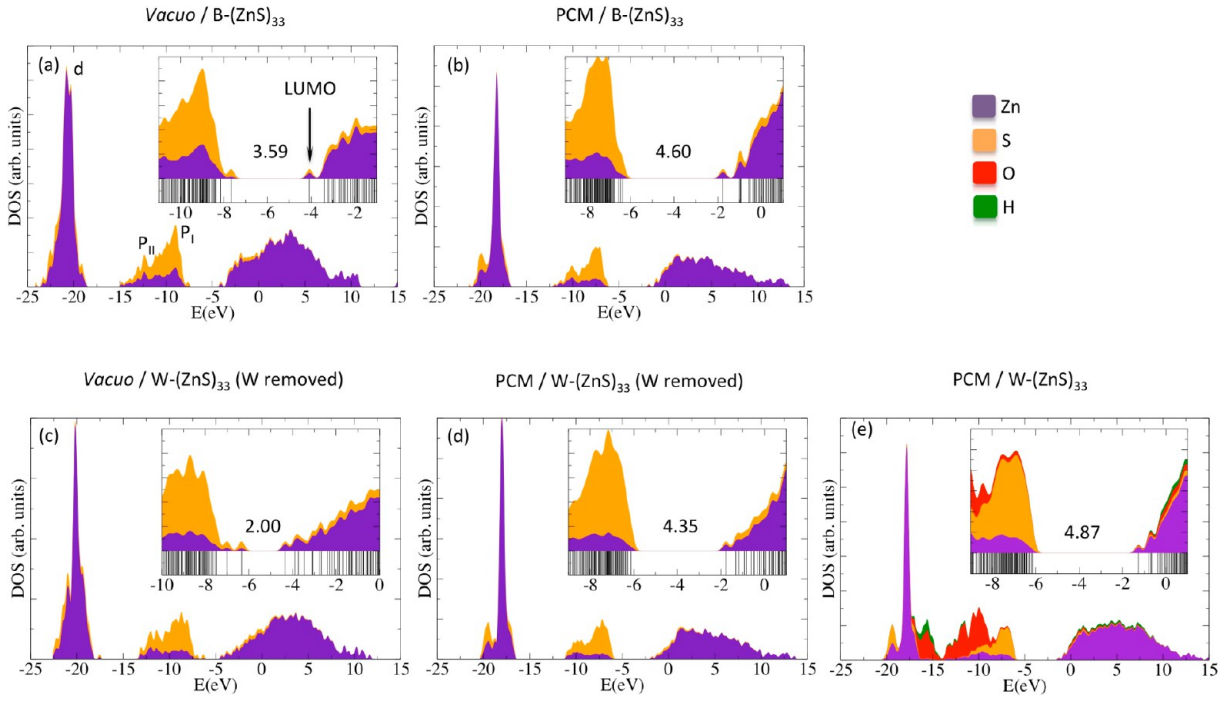

Figure 4. Total and projected density of states (DOS and PDOS) of B-$(ZnS)_{33}$ (a, b) and W-$(ZnS)_{33}$ (c, d, and e) obtained by a Gaussian convolution of σ = 0.20 eV of the individual KS orbitals. The insets display a zoom of the bandgap region. Results obtained at the B3LYP*/LANL2DZ level, calculated on top of the first equilibrated snapshot. Note that the contribution of each atom type is proportional to the colored area and not its height.

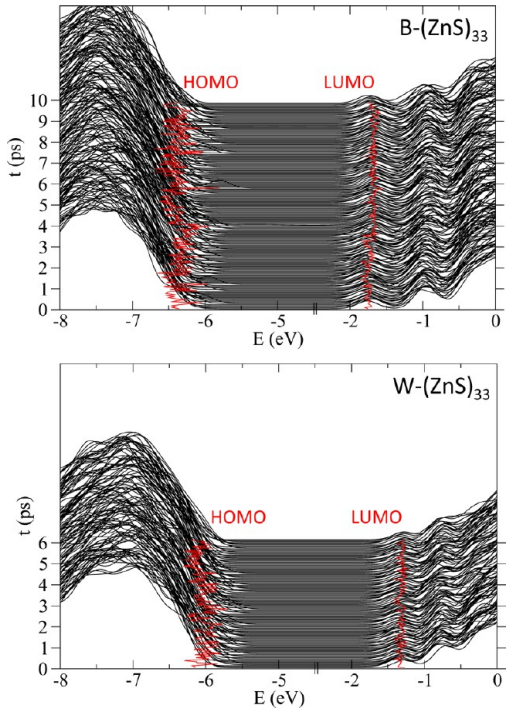

Figure 5. Density of states of B-$(ZnS)_{33}$ and W-$(ZnS)_{33}$, obtained by a Gaussian convolution of σ = 0.20 eV of the individual KS orbitals, along the dynamics. HOMO and LUMO levels highlighted in red.

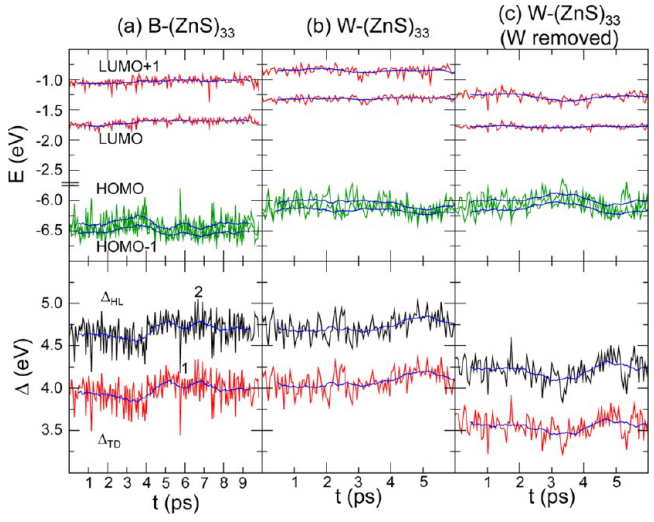

Figure 6. Top panels: KS energies of the frontier orbitals as a function of time for (a) B-$(ZnS)_{33}$, (b) W-$(ZnS)_{33}$, and (c) W-$(ZnS)_{33}$ after the removal of water molecules. Green and red lines stand for the occupied and virtual states, respectively. Bottom panels: Calculated HOMO−LUMO gaps, in black. The first TDDFT excitation energy is also provided, in red. Running averages in blue. Results obtained at the B3LYP*/LANL2DZ level.

Table S1, Supporting Information. To provide a direct comparison with B-$(ZnS)_{33}$, Zn−OH_2 and S−H_2O bonds have not been considered for the hydrated models. Zn and S atoms are assumed to be coordinated if the distance between them is smaller than 3.2 Å (the first minimum in the Zn−S RDF, see Figure 2). As one may notice from Figure S6, the Zn atoms are mainly 3-fold coordinated in B-$(ZnS)_{33}$, due to the large surface-to-volume ratio of the model. However, the number of 3-fold and 4-fold Zn atoms oscillates notably, reflecting the significant dynamical fluctuations of the bare QD. S atoms tend to be 3-coordinated. Nevertheless, the number of 3- and 4-fold S atoms fluctuates to a much lesser extent than variations in Zn coordination. In fact, transition metal atoms are

dx.doi.org/10.1021/jp409182r | J. Phys. Chem. C 2014, 118, 3274−3284

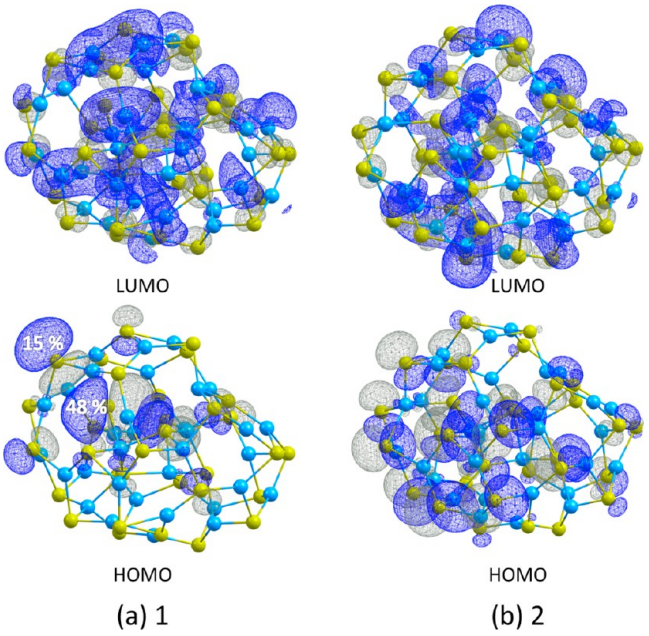

Figure 7. Isodensity plots of the frontier orbitals of two representative B-$(ZnS)_{33}$ structures, referred to as **1** and **2** in Figure 6. For visibility, contour value of 0.013 has been chosen. Light blue = Zn and yellow = S atoms.

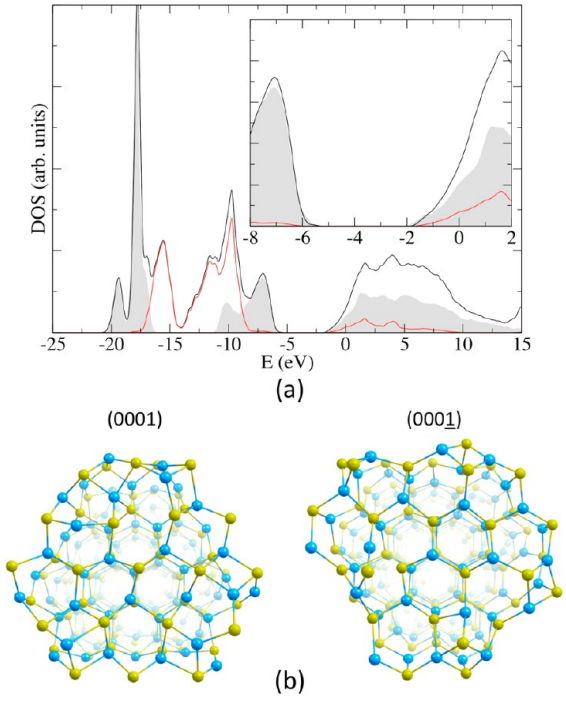

Figure 8. (a) Total (black line) and water-projected (red line) density of states of the W-$(ZnS)_{116}$, obtained by a Gaussian convolution of σ = 0.20 eV of the individual KS orbitals. For comparison, the DOS of the W-$(ZnS)_{116}$ after the removal of water molecules have been included (red, shaded). Results obtained at the B3LYP*/LANL2DZ level, averaged over four representative snapshots taken from the molecular dynamics. (b) Detail of the polar (0001) and (000$\bar{1}$) surfaces of the first equilibrated snapshot of W-$(ZnS)_{116}$. For clarity, water molecules are not shown. Light blue = Zn and yellow = S atoms.

obviously more versatile and can better accommodate different coordination environments. For the W-$(ZnS)_{33}$ model, 3-fold coordinated atoms are again more likely, but the differences with the 4-fold atoms are smaller. More importantly, the number of 3- and 4-fold oscillates to a lesser extent. Similar results have been obtained for the large W-$(ZnS)_{116}$ cluster. From this data, the structure of the bare cluster fluctuates notably, with several Zn−S bond breaking/forming over the time. Capping QDs surface with water molecules seems to lower the surface energy, stabilize the bulk-like geometry, and avoid Zn−S bond breaking events, which ultimately could lead to electronically localized midgap states

The Zn−Zn and S−S RDFs have also been calculated, see Figures S7 and S8, Supporting Information. The obtained Zn−Zn pair distributions roughly coincide with those reported for bubble and double-bubble ZnS nanoclusters,[61] with sharp peaks located at about 3.15 and 3.75 Å, which reflect the formation of square $(ZnS)_2$ and hexagonal $(ZnS)_3$ rings. Such 4- and 6-membered rings are recurrent motifs on the surface of II−VI semiconductor QDs and have been claimed to reduce the geometrical strain.[62] As found for Zn−S, the Zn−Zn and S−S distributions sharpen from B-$(ZnS)_{33}$ to W-$(ZnS)_n$ (n = 33, 116).

Let us now focus on the interaction between the QDs and the surrounding water solvent. There are presumably three ways for water adsorption on ZnS-QD surface:[20] (a) through Zn−O interactions; (b) through S−H interactions; or (c) through concomitant Zn−O and S−H interactions. To unravel the binding mode of water to the ZnS QDs, the Zn−O and S−H RDFs have been calculated, see Figure 3. Irrespective of the cluster size, average Zn−O and S−H distances of 2.08 and 2.28 Å have been obtained. These values commensurate with previous CPMD results for the hydrated $(ZnS)_4$ cluster,[20] with computed distances of 2.0 and 2.3 Å, respectively. Remarkably, the position of the first Zn−O peak essentially coincides with that measured experimentally for the hydrated Zn^{2+} cation (2.078 Å, as derived from EXAFS data analysis).[63] Regardless of the model, the Zn−O bond seems to be stronger than the S−H bond. The slightly shorter Zn−O distance for the smaller $(ZnS)_4$ cluster (2.0[20] vs 2.08 Å) could mean a stronger QD−water interaction, due to the enhanced nucleophilicity of the 2-fold coordinated Zn atoms in $(ZnS)_4$ compared to the 3-fold coordinated atoms on the surface of the $(ZnS)_{33}$ cluster. More recently, B3LYP/def2-TZVP results on hydrated $(ZnS)_4$ and $(ZnS)_6$ have also been reported, with calculated Zn−O distances increasing from 2.16 to 2.22 Å with increasing adsorption of water.[24]

The first feature in the Zn−O RDF represents the first layer of tightly bound water. For the W-$(ZnS)_{116}$ model, the area under the peak provides an average coordination number of 0.4 water molecules per Zn atom. The W-$(ZnS)_{33}$ model delivers a higher value of 0.5, meaning that the water coverage increases with the decreasing QD size, presumably due to the increased surface curvature of small QDs, which increases the surface reactivity and possibly minimizes the repulsion between adjacent adsorbed molecules.[20] In agreement with previous MD calculations regarding Zn^{2+} microsolvation,[64] our simulations discard the exchange of water molecules between the first and the second solvation shells. The minimum between the first and the second hydration spheres, located at $r \sim 3.0$ Å, is in agreement with previous MD simulations on the hydrated Zn^{2+} cation with a reported value of 2.85 Å.[65] The depth of this minimum is quite pronounced, implying a sizable energy penalty that prevents water exchange between the first and the second solvation shells. Our results are consistent with the long

dx.doi.org/10.1021/jp409182r | J. Phys. Chem. C 2014, 118, 3274−3284

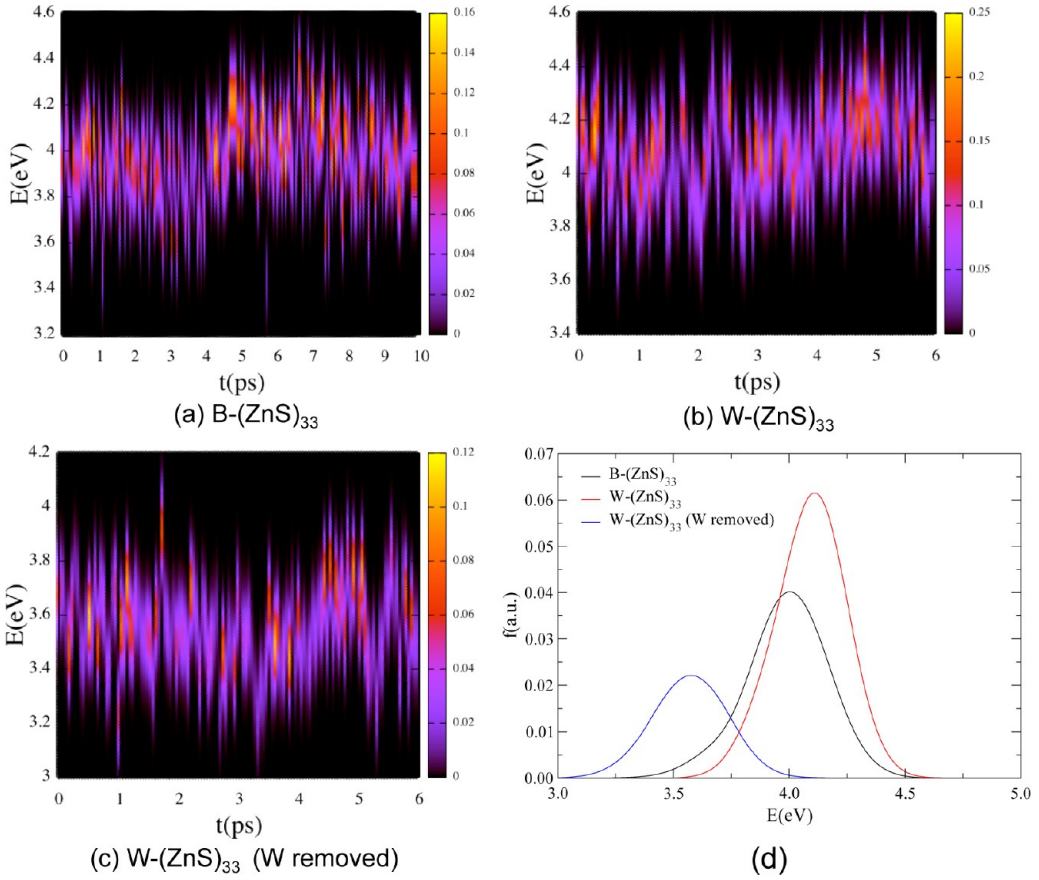

Figure 9. Absorption onset of (a) B-$(ZnS)_{33}$ and (b) W-$(ZnS)_{33}$ along the dynamics, drawn by a Gaussian convolution of the lowest TDDFT transition. *X* and *Y* axes correspond to the simulation time (in ps) and the excitation energy (in eV), respectively. Color scale refers to the oscillator strength, in a.u.. For completeness, the calculated onset of W-$(ZnS)_{33}$ structures after the removal of the water molecules is also shown in (c). Time-averaged spectra in (d). Results obtained at the B3LYP*/LANL2DZ level.

residence times reported for the microhydrated Zn^{2+} cation both experimentally and theoretically.[65]

In summary, ultrasmall bare clusters are predicted to exhibit large dynamic fluctuations at room temperature, and to undergo substantial structural rearrangements over time. Water molecules strongly interact with the QD surface by means of $Zn-OH_2$ bonds. Hydration lowers the surface energy and stabilizes the wurtzite-like geometry. Besides, bulk-like structures appear to be stabilized with the increasing size of the model, due to the decreased surface-to-volume ratio.

3.2. Electronic Properties. To model the optoelectronic properties of the investigated bare and hydrated QDs, single point DFT and excited state TDDFT calculations have been carried out on top of selected snapshot geometries taken from the CPMD simulation. As one may notice from Figure 4, where the Density of States (DOS) of the first production snapshot (t = 0 ps) is shown for each system, the B-$(ZnS)_{33}$ model displays a clear HOMO−LUMO gap of 3.59 eV, as calculated in the gas phase. Surface reconstruction leads to the saturation of the undercoordinated surface atoms, stabilizing the QD and, in principle, avoiding the occurrence of midgap states. The atomic orbitals projection of the DOS reveals that the high-lying occupied states (i.e., those constituting the valence band edge) arise mainly from S 3p orbitals, whereas the lowest-lying unoccupied states (i.e., those contributing the conduction band edge) are mainly composed by Zn 4s orbitals, see Figure S11, Supporting Information. Four main features are recognizable in the valence band of the B-$(ZnS)_{33}$ model, referred to as P_I, P_{II}, d, and P_{III} according to the notation proposed in the literature.[66] From the projected DOS, P_I and P_{III} are due to the S 3p and 3s orbitals, respectively. P_{II} arises from Zn 4s orbitals, with a notable participation of the S 3p states. Finally, the d feature is composed by Zn 3d orbitals. Our calculations qualitatively reproduce the valence band structure reported for the bulk material.[66] Notable differences are however found, that is, the calculated d band is located 13.09 eV below the top of the valence band, to be compared with the experimental value of about 9.0 eV. These differences are likely to be due to the small size of the QD, as they tend to be lifted by increasing the QD size.[25]

The inclusion of implicit water produces an upward shift of both the valence and the conduction band edges. The unoccupied states experience a larger solvent-induced energy displacement, so that the HOMO−LUMO gap sizably widens (4.60 eV). Implicit solvent stabilizes the outermost valence band states relative to the gas phase, thus, placing HOMO close to the other valence band orbitals. The LUMO, despite having a similar nature to the upper lying virtual orbitals, appears separated in energy from the rest of unoccupied orbitals. This observation coincides with our previous studies on Zn-based nanostructures[25,42,43] and with other theoretical works regarding CdSe,[67,68] revealing that this isolated LUMO might be an intrinsic property of the nanometric II−VI semiconductor materials.

For the hydrated clusters, calculations including CPCM as an additional implicit solvent layer improve the position of the

dx.doi.org/10.1021/jp409182r | J. Phys. Chem. C 2014, 118, 3274−3284

valence band features as compared to gas phase results so, unless otherwise stated, the CPCM results will be presented hereafter.

Moving to the hydrated W-$(ZnS)_{33}$ system, a wide HOMO−LUMO gap of 4.87 eV is calculated, see Figure 4e. The adsorption of explicit water molecules produces an upward displacement of both the valence and the conduction band edges, as recently found for anatase TiO_2 nanocrystals.[69] In our case, the conduction band experiences a larger shift, so that the HOMO−LUMO gaps opens by about 0.3 eV. Covering $(CdX)_n$ (X = Se, Te; n = 6, 9) nanoclusters with NH_3 and OPH_3 molecules has been calculated to cause a similar effect.[70] As observed for the B-$(ZnS)_{33}$ model, the HOMO is close to the rest of the occupied states and the LUMO is quite separated from the higher-lying unoccupied orbitals. The valence band features of ZnS are still recognizable in the W-$(ZnS)_{33}$ structure. Remarkably, the position of the bands remains almost unchanged. Water introduces occupied states between the P_I and the d bands. The molecular orbitals at about −10 eV reveal a significant hybridization between the Zn on the cluster surface and the O atoms of the water molecules, in line with the Zn−O adsorption mode proposed. The molecular orbitals at the edges of the valence and conduction bands are composed by S and Zn orbitals, respectively, as in the bare model. Consequently, the lowest-lying electronic transitions involve states localized in the $(ZnS)_{33}$ core, in agreement with previous results on hydrated $(ZnS)_n$ (n = 4, 6) clusters.[24]

To check whether the blue-shift of the band gap in the hydrated model arises from the geometry imposed by the solvation shell, the electronic structure of W-$(ZnS)_{33}$ after the removal of water molecules has also been calculated, see Figure 4d. The shape of the valence and conduction band edges remains almost unchanged. However, the structural distortion is predicted to produce a significant reduction of the HOMO−LUMO, with a computed value by CPCM of 4.35 eV. Zwijnenburg et al. observed a similar effect in their work regarding small hydrated ZnS clusters, where the electrostatic field induced by the absorbed water molecules was proven to be responsible for the opening of the gap.[24] Not only the electric field, but also the electron-donor properties of the H_2O molecules may however play a role. Indeed, the W-$(ZnS)_{33}$ has been calculated to bear a formal charge of about −4 |e| due to the charge transfer from the solvent molecules to the QD. For completeness, gas phase results of the W-$(ZnS)_{33}$ after the removal of water molecules are also reported. Calculations deliver a HOMO−LUMO gap of 2.00 eV, due to the appearance of occupied midgap states.

Figure 5 shows the evolution of the band-edge state density along the dynamics for the B-$(ZnS)_{33}$ and W-$(ZnS)_{33}$ models. Irrespective of the model, the LUMO remains almost constant along the whole CPMD trajectory. On the contrary, the HOMO energy oscillates notably. Such fluctuations are particularly important for B-$(ZnS)_{33}$. As one may notice from Figure 6, the bare model exhibits wide HOMO−LUMO gaps of about 4.5−5.0 eV. However, eventually the band gap shrinks due to the appearance of high-lying HOMOs, separated from the rest of the valence band states. To elucidate the nature of such midgap states, the projection of the band edges orbitals on the basis functions of the individual atoms have been calculated, see Table S2 and Figure S12, Supporting Information. The dispersion of the individual contributions of the cluster atoms to the molecular orbitals, quantified by means of the standard deviation of the distribution, provides a sketch of the localization of the molecular orbital. From our calculations, the low-lying unoccupied orbitals are much more delocalized than the high-lying occupied orbitals, irrespective of the model and of the considered snapshot. The HOMOs are particularly localized in the case of the bare B-$(ZnS)_{33}$ model. To better illustrate this point, the B-$(ZnS)_{33}$ structure with the highest HOMO (and lowest band gap) has been analyzed in detail, see **1** in Figure 6. For comparison, the snapshot with the lowest HOMO (and highest band gap) has also been considered, see **2** in Figure 6. As it appears, the frontier orbitals of structures **1** and **2** show significant differences, see Figure 7. For structure **2**, both the HOMO and the LUMO are delocalized over the entire cluster. For structure **1**, the LUMO is also spread over the whole QD, whereas the HOMO is mainly concentrated on two S atoms, that is, a 2-fold coordinated core atom and a three-coordinated surface atom. For structure **1**, the S atoms highlighted in Figure 7a comprise 48 and 15% of the HOMO, respectively. On the contrary, the HOMO of structure **2** is distributed over all the 33 S atoms in the nanostructure, with no individual contribution larger than 10%. From our calculations, the break-up of Zn−S bonds and the formation of under-coordinated S atoms may thus result in the appearance of midgap states above the valence band edge, with the concomitant shrinkage of the band gap. The inclusion of the explicit solvent has important consequences, limiting bond breaking phenomena and consequently hindering the emergence of high-lying localized states.

Regarding the W-$(ZnS)_{116}$ model, the average DOS of representative snapshots has been calculated, along with the projection on the water molecules, see Figure 8. This hydrated model displays a HOMO−LUMO gap of 4.38 eV, ∼0.5 eV smaller than W-$(ZnS)_{33}$. However, the shape of the valence band is almost the same. Remarkably, the highest-lying occupied orbitals are quite separated from the rest of the valence band states. Such states have been found to arise from S atoms in the polar surfaces of the $(ZnS)_{116}$ cluster. Therefore, the solvent cannot totally avoid the occurrence of localized states on the ZnS polar surfaces. For comparison, the DOS of the same structure after the removal of the solvent molecules is also shown. The shape of the valence and conduction band edges does not change significantly. However, the band gap slightly decreases with respect to the hydrated model (4.13 vs 4.38 eV) due to the downward shift of the LUMOs. From Figure 8, the water-related states are predicted to intrude between the P_{II} and d features of the ZnS QD, as calculated for the W-$(ZnS)_{33}$ model.

3.3. Optical Properties. Even if the Kohn−Sham (KS) eigenvalues provide reasonable values for the band gap transition energies of bulk II−VI semiconductors, the description of the excitons in nanostructures requires a more rigorous groundwork, as that supplied by TDDFT.[71] Therefore, Figure 9 the simulated absorption onset of B-$(ZnS)_{33}$ and W-$(ZnS)_{33}$, obtained by a Gaussian convolution of the lowest TDDFT transition calculated for each system, sampled along the dynamics trajectory. For the bare model the optical gap emerges at 4.0 eV, in line with the experimental results reported for small ZnS nanoparticles.[72−74] As previously noticed, water adsorption leads to a slight absorption blue-shift of 0.1−0.2 eV. Furthermore, the intensity of the lowest transition is found to increase, in agreement with previous works.[24] Irrespective of the model, the LUMO is the final state of the lowest-lying TDDFT excitations. Since the cooling of the photogenerated hole to the HOMO is expected to occur rapidly by virtue of the

dx.doi.org/10.1021/jp409182r | J. Phys. Chem. C 2014, 118, 3274−3284

large effective mass of the hole and the high valence band DOS, our models are predicted to display sharp emission bands, related to the LUMO − HOMO relaxation. Eventually, the B-$(ZnS)_{33}$ model displays low-intensity absorption features in the low-energy region of the spectrum. These signatures are related to the localized HOMOs, as discussed above, and tend to disappear upon hydration.

4. SUMMARY AND CONCLUSIONS

The effect of structure and solvent dynamics on the optoelectronic properties of realistic ZnS QDs has been studied. Inclusion of explicit water molecules in our simulations plays an important role on the structure of the investigated QDs by lowering the surface energy and stabilizing a bulk-like geometry, thus, avoiding the occurrence of Zn−S bond breaking events.[19] Hydration produces in all cases an upward shift of both the valence and the conduction band edges, which ultimately leads to a blue-shift of about 0.3 eV of the absorption onset. The electrostatic field induced by the solvent shell and the electron-donor properties of the water molecules are supposed to be responsible for the opening of the gap. Besides, covering the QD with water increases the intensity of the low-lying electronic excitations.

The dynamic behavior of the ZnS QDs is reflected in their optoelectronic properties. The band-edge states vary continuously along the CPMD trajectory. For the bare $(ZnS)_{33}$ model, eventually the band gap shrinks due to the appearance of high-lying HOMOs, segregated from the rest of the valence band states. These high-lying states have been shown to be localized in nature. From our simulations, the continuous Zn−S bond breaking observed in the bare model leads to such midgap states, which could act as trap states. The inclusion of the explicit solvent appears to stabilize the wurtzite-like geometry, prevent the bond disruption and hinder the emergence of S-localized high-lying states.

This study sheds light on the important optoelectronic modifications occurring for realistic QDs in water solution and further provides the methodological framework to investigate photocatalytic reactions mediated by ZnS.

■ ASSOCIATED CONTENT

Supporting Information

Additional graphs and tables and full references 38 and 54. This material is available free of charge via the Internet at http://pubs.acs.org.

■ AUTHOR INFORMATION

Corresponding Author

*E-mail: filippo@thch.unipg.it. Tel.: +390755855523.

Notes

The authors declare no competing financial interest.

■ ACKNOWLEDGMENTS

This research was funded by Eusko Jaurlaritza/Basque Government (IT588-13 and S-PC12UN003) and the Spanish Office for Scientific Research (CTQ2012-38496-C05-01). The SGI/IZO-SGIker UPV/EHU is gratefully acknowledged for generous allocation of computational resources. J.M.A. would like to thank the Spanish Ministry of Education for funding through a FPU fellowship (AP2009-1514). E.M. and F.D.A. thank FP7-ENERGY-2010 Project "ESCORT" (261920) and CNR-EFOR for financial support.

■ REFERENCES

(1) Alivisatos, A. P. Perspectives on the Physical Chemistry of Semiconductor Nanocrystals. *J. Phys. Chem.* **1996**, *100*, 13226−13239.
(2) Alivisatos, A. P. Semiconductor Clusters, Nanocrystals, and Quantum Dots. *Science* **1996**, *271*, 933−937.
(3) Hetsch, F.; Xu, X.; Wang, H.; Kershaw, S. V.; Rogach, A. L. Semiconductor Nanocrystal Quantum Dots as Solar Cell Components and Photosensitizers: Material, Charge Transfer, and Separation Aspects of Some Device Topologies. *J. Phys. Chem. Lett.* **2011**, *2*, 1879−1887.
(4) Kamat, P. V. Quantum Dot Solar Cells. Semiconductor Nanocrystals as Light Harvesters. *J. Phys. Chem. C* **2008**, *112*, 18737−18753.
(5) Abbasi, A. Z.; Amin, F.; Niebling, T.; Friede, S.; Ochs, M.; Carregal-Romero, S.; Montenegro, J.-M.; Rivera Gil, P.; Heimbrodt, W.; Parak, W. J. How Colloidal Nanoparticles Could Facilitate Multiplexed Measurements of Different Analytes with Analyte-sensitive Organic Fluorophores. *ACS Nano* **2011**, *5*, 21−5.
(6) Jimenez De Aberasturi, D.; Montenegro, J. M.; Ruiz De Larramendi, I.; Rojo, T.; Klar, T. A.; Alvarez-Puebla, R.; Liz-Marza, L. M.; Parak, W. J. Optical Sensing of Small Ions with Colloidal Nanoparticles. *Chem. Mater.* **2012**, *24*, 738−745.
(7) Nann, T.; Skinner, W. M. Quantum Dots for Electro-Optic Devices. *ACS Nano* **2011**, *5*, 5291−5295.
(8) Harris, C.; Kamat, P. V. Photocatalysis with CdSe Nanoparticles in Confined Media: Mapping Charge Transfer Events in the Subpicosecond to Second Timescales. *ACS Nano* **2009**, *3*, 682−90.
(9) Harris, C.; Kamat, P. V. Photocatalytic Events of CdSe Quantum Dots in Confined Media. Electrodic Nanoparticles. *ACS Nano* **2010**, *4*, 7321−7330.
(10) Ruberu, T. P. a.; Nelson, N. C.; Slowing, I. I.; Vela, J. Selective Alcohol Dehydrogenation and Hydrogenolysis with Semiconductor-Metal Photocatalysts: Toward Solar-to-Chemical Energy Conversion of Biomass-Relevant Substrates. *J. Phys. Chem. Lett.* **2012**, *3*, 2798−2802.
(11) Wang, C.; Thompson, R. L.; Baltrus, J.; Matranga, C. Visible Light Photoreduction of CO_2 Using CdSe/Pt/TiO_2 Heterostructured Catalysts. *J. Phys. Chem. Lett.* **2010**, *1*, 48−53.
(12) Fang, X.; Bando, Y.; Gautam, U. K.; Zhai, T.; Zeng, H.; Xu, X.; Liao, M.; Golberg, D. ZnO and ZnS Nanostructures: Ultraviolet-Light Emitters, Lasers, and Sensors. *Crit. Rev. Solid State Mater. Sci.* **2009**, *34*, 190−223.
(13) Chen, D.; Huang, F.; Ren, G.; Li, D.; Zheng, M.; Wang, Y.; Lin, Z. ZnS Nano-Architectures: Photocatalysis, Deactivation, and Regeneration. *Nanoscale* **2010**, *2*, 2062−4.
(14) Medintz, I. L.; Uyeda, H. T.; Goldman, E. R.; Mattoussi, H. Quantum Dot Bioconjugates for Imaging, Labelling and Sensing. *Nat. Mater.* **2005**, *4*, 435−446.
(15) Feigl, C.; Russo, S. P.; Barnard, A. S. Safe, Stable and Effective Nanotechnology: Phase Mapping of ZnS Nanoparticles. *J. Mater. Chem.* **2010**, *20*, 4971−4980.
(16) Gilbert, B.; Huang, F.; Lin, Z.; Goodell, C.; Zhang, H.; Banfield, J. F. Surface Chemistry Controls Crystallinity of ZnS Nanoparticles. *Nano Lett.* **2006**, *6*, 605−10.
(17) Gilbert, B.; Zhang, H.; Huang, F.; Banfield, J. F.; Ren, Y.; Haskel, D.; Lang, J. C.; Srajer, G.; Jürgensen, A.; Waychunas, G. A. Analysis and Simulation of the Structure of Nanoparticles that Undergo a Surface-Driven Structural Transformation. *J. Chem. Phys.* **2004**, *120*, 11785−11795.
(18) Goodell, C. M.; Gilbert, B.; Weigand, S. J.; Banfield, J. F. Kinetics of Water Adsorption-Driven Structural Transformation of ZnS Nanoparticles. *J. Phys. Chem. C* **2008**, *112*, 4791−4796.
(19) Zhang, H.; Gilbert, B.; Huang, F.; Banfield, J. F. Water-Driven Structure Transformation in Nanoparticles at Room Temperature. *Nature* **2003**, *424*, 1025−1029.
(20) Zhang, H.; Rustad, J. R.; Banfield, J. F. Interaction between Water Molecules and Zinc Sulfide nanoparticles Studied by Temperature-Programmed Desorption and Molecular Dynamics Simulations. *J. Phys. Chem. A* **2007**, *111*, 5008−5014.

(21) Chen, H. M.; Chen, C. K.; Liu, R.-S.; Wu, C.-C.; Chang, W.-S.; Chen, K.-H.; Chan, T.-S.; Lee, J.-F.; Tsai, D. P. A New Approach to Solar Hydrogen Production: a ZnO−ZnS Solid Solution Nanowire Array Photoanode. *Adv. Energy Mater.* **2011**, *1*, 742−747.
(22) Tachibana, Y.; Vayssieres, L.; Durrant, J. R. Artificial Photosynthesis for Solar Water-Splitting. *Nat. Photonics* **2012**, *6*, 511−518.
(23) Zwijnenburg, M. A. Photoluminescence in Semiconductor Nanoparticles: an Atomistic View of Excited State Relaxation in Nanosized ZnS. *Nanoscale* **2012**, *4*, 3711−3717.
(24) Zwijnenburg, M. A.; Illas, F.; Bromley, S. T. The Fate of optical Excitations in Small Hydrated ZnS Clusters: a Theoretical Study into the Effect of Hydration on the Excitation and Localisation of Electrons in Zn4S4 and Zn6S6. *Phys. Chem. Chem. Phys.* **2011**, *13*, 9311−9317.
(25) Azpiroz, J. M.; Mosconi, E.; De Angelis, F. Modeling ZnS and ZnO Nanostructures: Structural, Electronic, and Optical Properties. *J. Phys. Chem. C* **2011**, *115*, 25219−25226.
(26) Pennycook, T. J.; McBride, J. R.; Rosenthal, S. J.; Pennycook, S. J.; Pantelides, S. T. Dynamic Fluctuations in Ultrasmall Nanocrystals Induce White Light Emission. *Nano Lett.* **2012**, *12*, 3038−3042.
(27) Voznyy, O. Mobile Surface Traps in CdSe Nanocrystals with Carboxylic Acid Ligands. *J. Phys. Chem. C* **2011**, 15927−15932.
(28) Voznyy, O.; Thon, S. M.; Ip, A. H.; Sargent, E. H. Dynamic Trap Formation and Elimination in Colloidal Quantum Dots. *J. Phys. Chem. Lett.* **2013**, *4*, 987−992.
(29) Kasuya, A.; Sivamohan, R.; Barnakov, Y. A.; Dmitruk, I. M.; Nirasawa, T.; Romanyuk, V. R.; Kumar, V.; Mamykin, S. V.; Tohji, K.; Jeyadevan, B.; Shinoda, K.; Kudo, T.; Terasaki, O.; Liu, Z.; Belosludov, R. V.; Sundararajan, V.; Kawazoe, Y. Ultra-Stable Nanoparticles of CdSe Revealed from Mass Spectrometry. *Nat. Mater.* **2004**, 3, 99−102.
(30) Botti, S.; Marques, M. Identification of Fullerene-Like CdSe Nanoparticles from Optical Spectroscopy Calculations. *Phys. Rev. B* **2007**, *75*, 1−6.
(31) Kasuya, A.; Noda, Y.; Dmitruk, I.; Romanyuk, V.; Barnakov, Y.; Tohji, K.; Kumar, V.; Belosludov, R.; Kawazoe, Y.; Ohuchi, N. Stoichiometric and Ultra-Stable Nanoparticles of II-VI Compound Semiconductors. *Eur. Phys. J. D* **2005**, *34*, 39−41.
(32) Kilina, S.; Ivanov, S.; Tretiak, S. Effect of Surface Ligands on Optical and Electronic Spectra of Semiconductor Nanoclusters. *J. Am. Chem. Soc.* **2009**, *131*, 7717−7726.
(33) Puzder, A.; Williamson, A. J.; Gygi, F.; Galli, G. Self-Healing of CdSe Nanocrystals: First-Principles Calculations. *Phys. Rev. Lett.* **2004**, *92*, 217401(1−4).
(34) Perdew, J. P.; Burke, K.; Ernzerhof, M. Generalized Gradient Approximation Made Simple. *Phys. Rev. Lett.* **1996**, *77*, 3865−3868.
(35) Velde, G. T.; Bickelhaupt, F. M.; Baerends, E. J.; Guerra, C. F.; Gisbergen, S. J. A. V.; Snijders, J. G.; Ziegler, T. Chemistry with ADF. *J. Comput. Chem.* **2001**, *22*, 931−967.
(36) Car, R.; Parrinello, M. Unified Approach for Molecular Dynamics and Density-Functional Theory. *Phys. Rev. Lett.* **1985**, *55*, 2471−2474.
(37) Giannozzi, P.; De Angelis, F.; Car, R. First-Principle Molecular Dynamics with Ultrasoft Pseudopotentials: Parallel Implementation and Application to Extended Bioinorganic Systems. *J. Chem. Phys.* **2004**, *120*, 5903−5915.
(38) Giannozzi, P.; Baroni, S.; Bonini, N.; Calandra, M.; Car, R.; Cavazzoni, C.; Ceresoli, D.; Chiarotti, G. L.; Cococcioni, M.; Dabo, I.; et al. QUANTUM ESPRESSO: a Modular and Open-Source Software Project for Quantum Simulations of Materials. *J. Phys.: Condens. Matter* **2009**, *21*, 395502(1−19).
(39) Hay, P. J.; Wadt, W. R. Ab Initio Effective Core Potentials for Molecular Calculations. Potentials for K to Au Including the Outermost Core Orbitals. *J. Chem. Phys.* **1985**, *82*, 299−310.
(40) Hay, P. J.; Willard, R. W. Ab Initio Effective CorePotentials for Molecular Calculations. Potentials for the Transition Metal Atoms Sc to Hg. *J. Chem. Phys.* **1985**, *82*, 270−283.
(41) Wadt, W. R.; Hay, P. J. Ab Initio Effective Core Potentials for Molecular Calculations. Potentials for Main Group Elements Na to Bi. *J. Chem. Phys.* **1985**, *82*, 284−298.
(42) De Angelis, F.; Armelao, L. Optical Properties of ZnO Nanostructures: a Hybrid DFT/TDDFT Investigation. *Phys. Chem. Chem. Phys.* **2011**, *13*, 467−475.
(43) Azpiroz, J. M.; Infante, I.; Lopez, X.; Ugalde, J. M.; De Angelis, F. A First-Principles Study of II−VI (II = Zn; VI = O, S, Se, Te) Semiconductor Nanostructures. *J. Mater. Chem.* **2012**, *22*, 21453−21465.
(44) Azpiroz, J. M.; Matxain, J. M.; Infante, I.; Lopez, X.; Ugalde, J. M. A DFT/TDDFT Study on the Optoelectronic Properties of the Amine-Capped Magic $(CdSe)_{13}$ Nanocluster. *Phys. Chem. Chem. Phys.* **2013**, *15*, 10996−11005.
(45) Nguyen, K. A.; Day, P. N.; Pachter, R. Understanding Structural and Optical Properties of Nanoscale CdSe Magic-Size Quantum Dots: Insight from Computational Prediction. *J. Phys. Chem. C* **2010**, *114*, 16197−16209.
(46) Azpiroz, J. M.; Ugalde, J.; Infante, I. Benchmark Assessment of Density Functional Methods on Group II−VI MX (M = Zn, Cd; X = S, Se, Te) Quantum Dots. *J. Chem. Theor. Comp.* **2014**, *10*, 76−89.
(47) Dolg, M.; Wedig, U.; Stoll, H.; Preuss, H. Energy-Adjusted Ab Initio Pseudopotentials for the First Row Transition Elements. *J. Chem. Phys.* **1987**, *86* (2), 866−872.
(48) Dunning, T. H.; Hay, P. J. In *Modern Theoretical Chemistry*; Schaefer ,H. F., III, Ed.; Plenum: New York, 1976; Vol. *3*, pp 1−28.
(49) Andrade, D.; Häubermann, U.; Dolg, M.; Stoll, H.; Preub, H. Energy-Adjusted Ab Initio Pseudopotentials for the Second and Third Row Transition Elements. *Theor. Chim. Acta* **1990**, *77*, 123−141.
(50) Weigend, F.; Ahlrichs, R. Balanced Basis Sets of Split Valence, Triple Zeta Valence and Quadruple Zeta Valence Quality for H to Rn: Design and Assessment of Accuracy. *Phys. Chem. Chem. Phys.* **2005**, *7*, 3297−3305.
(51) Cossi, M.; Rega, N.; Scalmani, G.; Barone, V. Energies, Structures, and Electronic Properties of Molecules in Solution with the C-PCM Solvation Model. *J. Comput. Chem.* **2003**, *24*, 669−681.
(52) Cossi, M.; Barone, V. Separation between Fast and Slow Polarizations in Continuum Solvation Models. *J. Phys. Chem. A* **2000**, *104*, 10614−10622.
(53) Cossi, M.; Barone, V. Time-Dependent Density Functional Theory for Molecules in Liquid Solutions. *J. Chem. Phys.* **2001**, *115*, 4708−4717.
(54) Frisch, M. J.; Trucks, G. W.; Schlegel, H. B.; Scuseria, G. E.; Robb, M. A.; Cheeseman, J. R.; Scalmani, G.; Barone, V.; Mennucci, B.; Petersson et al., *Gaussian 09*, Revision B.01.; Gaussian, Inc.: Wallingford, CT, 2009.
(55) Humphrey, W.; Dalke, A.; Schulten, K. VMD - Visual Molecular Dynamics. *J. Mol. Graphics* **1996**, *14*, 33−38.
(56) Macrae, C. F.; Edgington, P. R.; McCabe, P.; Pidcock, E.; P., S. G.; Taylor, R.; Towler, M.; van de Streek, J. Mercury: Visualization and Analysis of Crystal Structures. *J. Appl. Crystallogr.* **2006**, *39*, 453−457.
(57) Junkermeier, C.; Lewis, J.; Bryant, G. Amorphous Nature of Small CdS Nanoparticles: Molecular Dynamics Simulations. *Phys. Rev. B* **2009**, *79*, 125323(1−8).
(58) Jose, R.; Zhanpeisov, N. U.; Fukumura, H.; Baba, Y.; Ishikawa, M. Structure-Property Correlation of CdSe Clusters Using Experimental Results and First-Principles DFT Calculations. *J. Am. Chem. Soc.* **2006**, *128*, 629−636.
(59) Zhang, J.; Jin, S.; Fry, H. C.; Peng, S.; Shevchenko, E.; Wiederrecht, G. P.; Rajh, T. Synthesis and Characterization of Wurtzite ZnTe Nanorods with Controllable Aspect Ratios. *J. Am. Chem. Soc.* **2011**, *133*, 15324−15327.
(60) Goswami, N.; Sen, P. Water-Induced Stabilization of ZnS Nanoparticles. *Solid State Commun.* **2004**, *132*, 791−794.
(61) Hamad, S.; Catlow, C. R. A.; Spanò, E.; Matxain, J. M.; Ugalde, J. M. Structure and Properties of ZnS Nanoclusters. *J. Phys. Chem. B* **2005**, *109*, 2703−2709.
(62) Matxain, J. M.; Mercero, J. M.; Fowler, J. E.; Ugalde, J. M. Clusters of II−VI Materials: CdiXi, X = S, Se, Te, $i \leq 16$. *J. Phys. Chem. A* **2004**, *108*, 10502−10508.

(63) D'Angelo, P.; Barone, V.; Chillemi, G.; Sanna, N.; Meyer-Klaucke, W.; Pavel, N. V. Hydrogen and Higher Shell Contributions in Zn^{2+}, Ni^{2+}, and Co^{2+} Aqueous Solutions: an X-Ray Absorption Fine Structure and Molecular Dynamics Study. *J. Am. Chem. Soc.* **2002**, *124*, 1958−1967.
(64) Hamad, S.; Cristol, S.; Catlow, C. R. a. Simulation of the Embryonic Stage of ZnS Formation from Aqueous Solution. *J. Am. Chem. Soc.* **2005**, *127*, 2580−2590.
(65) Wu, J. C.; Piquemal, J.-P.; Chaudret, R.; Reinhardt, P.; Ren, P. Polarizable Molecular Dynamics Simulation of Zn(II) in Water Using the AMOEBA Force Field. *J. Chem. Theory Comput.* **2010**, *6*, 2059−2070.
(66) Ley, L.; Pollak, R. A.; McFeely, F. R.; Kowalczyk, S. P.; Shirley, D. A. Total Valence-Band Densities of States of III−V and II−VI Compounds from X-Ray Photoemission Spectroscopy. *Phys. Rev. B* **1974**, *9*, 600−621.
(67) Del Ben, M.; Havenith, R. W. A.; Broer, R.; Stener, M. Density Functional Study on the Morphology and Photoabsorption of CdSe Nanoclusters. *J. Phys. Chem. C* **2011**, *115*, 16782−16796.
(68) Wang, L. W.; Zunger, A. Pseudopotential Calculations of Nanoscale CdSe Quantum Dots. *Phys. Rev. B* **1996**, *53*, 9579−9582.
(69) Nunzi, F.; Mosconi, E.; Storchi, L.; Ronca, E.; Selloni, A.; Gratzel, M.; De Angelis, F. Inherent Electronic Trap States in TiO_2 Nanocrystals: Effect of Saturation and Sintering. *Energy Environ. Sci.* **2013**, *6*, 1221−1229.
(70) Kuznetsov, A. E.; Balamurugan, D.; Skourtis, S. S.; Beratan, D. N. Structural and Electronic Properties of Bare and Capped Cd_nSe_n/Cd_nTe_n Nanoparticles (n = 6, 9). *J. Phys. Chem. C* **2012**, *116*, 6817−6830.
(71) Matxain, J. M.; Mercero, J. M.; Fowler, J. E.; Ugalde, J. M. Electronic Excitation Energies of Zn_iO_i Clusters. *J. Am. Chem. Soc.* **2003**, *125*, 9494−9499.
(72) Biswas, S.; Kar, S. Fabrication of ZnS Nanoparticles and Nanorods with Cubic and Hexagonal Crystal Structures: a Simple Solvothermal Approach. *Nanotechnology* **2008**, *19*, 45710(1−11).
(73) Souici, A. H.; Keghouche, N.; Delaire, J. A.; Remita, H.; Mostafavi, M. Radiolytic Synthesis and Optical Properties of Ultra-Small Stabilized ZnS Nanoparticles. *Chem. Phys. Lett.* **2006**, *422*, 25−29.
(74) Zhao, Y.; Zhang, Y.; Zhu, H.; Hadjipanayis, G. C.; Xiao, J. Q. Low-Temperature Synthesis of Hexagonal (Wurtzite) ZnS Nanocrystals. *J. Am. Chem. Soc.* **2004**, *126*, 6874−6875.